Meccanica
DOI 10.1007/s11012-016-0461-8

Bifurcation and pull-in voltages of primary resonance of electrostatically actuated SWCNT cantilevers to include van der Waals effect

Dumitru I. Caruntu · Le Luo

Received: 8 October 2015 / Accepted: 23 May 2016

Abstract In this work the voltage response of primary resonance of electrostatically actuated single wall carbon nano tubes (SWCNT) cantilevers over a parallel ground plate is investigated. Three forces act on the SWCNT cantilever, namely electrostatic, van der Waals and damping. While the damping is linear, the electrostatic and van der Waals forces are nonlinear. Moreover, the electrostatic force is also parametric since it is given by AC voltage. Under these forces the dynamics of the SWCNT is nonlinear parametric. The van der Waals force is significant for values less than 50 nm of the gap between the SWCNT and the ground substrate. Reduced order model method (ROM) is used to investigate the system under soft excitation and weak nonlinearities. The voltage-amplitude response and influences of parameters are reported for primary resonance (AC near half natural frequency).

Keywords SWCNT resonators · Primary resonance · Voltage response

D. I. Caruntu (✉) · L. Luo
Mechanical Engineering Department, University of Texas-Rio Grande Valley, Edinburg, TX 78541, USA
e-mail: dumitru.caruntu@utrgv.edu;
caruntud2@asme.org;
dcaruntu@yahoo.com

1 Introduction

Carbon nanotubes (CNTs) have been discovered in 1991, and since then they have generated scientific and technological interest due to their attractive physical characteristics, high durability and light weight relative to metals, CNTs are formed by strong carbon-to-carbon covalent bonds [35] and they are high-aspect-ratio structures. CNTs exhibit enhanced electrical characteristics in comparison with most other conductive materials, and has the potential for a defect-free structure and the strongest material that has ever been discovered [35]. The actual magnitude of these properties depends on the diameter and chirality of the nanotubes along with the number of walls [24].

Applications of CNTs as ideal mechanical components are in the areas of mass sensors, nano-switches, and resonators. Their exceptional mass-detecting capability makes them excellent "mass spectrometers." CNTs mass sensing applications can be separated into two categories: chemical sensors and biosensors [27]. Sensitivity of resonator sensors is given by their effective vibratory mass and their natural frequencies, and it is affected by nonlinearities in the system. The principle of resonator sensors consists of their natural frequency shift due to additional mass that attaches to the resonator. Usually the fundamental mode of vibration is used for sensing. Both, the additional mass and its location on the sensor change its dynamic response. CNTs' excellent sensitivity is due to (1) their low weight, a tiny addition of atoms will

Published online: 21 June 2016

represent a large fraction of the overall weight, and (2) the fact that CNTs are ultra-rigid, having extremely high fundamental resonant frequency. The added mass can be either a point mass or a homogeneous layer covering the full length of the CNT. To determine at which point along the cantilever the mass was added, a method of measuring the resonant frequencies of the beam without and with varied added masses for several vibration modes was developed [33].

Models and results of CNT sensors were reported in the literature. There are four main models to investigate the mechanical behaviors of nanostructures: quantum mechanics, atomistic simulation, continuum modeling, and lumped system modeling. Yet due to the complex nature of these models, the most commonly seen model involves classic beam theory [17] to eventualy include nonlocal effects [22]. Models of CNT cantilevers as a spring with nanoscale mass attached to the free end were reported in the literature [34]. The results showed a good agreement with theoretical and experimental data reported in the literature. The two positions of attached mass on the CNTs resulted in two different nonlinear characteristics, namely softening and hardening effects. Chowdhury and Adhikari [12] investigated two different cases (1) fixed-free (cantilever) CNTs with mass attached to the free end, and (2) fixed–fixed (bridge) CNTs with mass attached at the midpoint. By changing the mass, the frequency shift occurred in a smaller range in the bridge case than that in cantilever case. Mehdipour et al. [27] indicated for cantilevers that the increase of the amount and the distance from the fixed edge of the attached mass resulted in a decrease of the dynamic pull-in voltage if electrostatically actuated. The mass sensitivity increased as the mass was moved towards the tip of the cantilever. Georgantznos and Anifantis [18] utilized a spring–mass-based finite element formulation for investigating single- and multi-walled carbon nanotube dynamics. They showed that the frequency shift is almost constant in several basic vibrational modes independent of the location of the added mass to the CNT.

Electrostatically actuated CNT is a beam structure in capacitive arrangement with a parallel plate electrode, or placed between a pair of parallel plate electrodes. The CNT is driven by DC and AC voltages between the CNT and plate electrode or electrodes [3]. The deflection of carbon nanotubes occurs under the attractive electrostatic and van der Waals forces. The CNT electrode deflects up to where its elastic force balances the attractive forces. Beyond a critical voltage or frequency the CNT electrode loses stability and suddenly drops on the fixed electrode. This is called pull-in phenomenon. This phenomenon is used for switches, capacitors, and resonators [16]. Caruntu and Luo [7] reported the frequency response of primary resonance of electrostatically actuated CNTs.

Nano-electromechanical systems (NEMS) include CNT nano-switches. They have the capability of offering high resonant frequencies in the gigahertz range, and the advantage of low energy consumption [27]. Yet, because of their size, these nano-electromechanical systems have a low output signal level [1]. These switches are designed as CNT suspended over a parallel ground electrode. The applied voltage across the CNT and rigid plate has an upper limit, beyond which the CNT collapses on the ground plate. This voltage limit is called the "pull-in voltage" [27] and depends upon the gap-length ration of the CNT, as well as frequency of actuation if AC electrostatically actuated. The dominant approach in the investigation of pull-in behaviors of electrostatically actuated NEMS in general, and CNTs in particular, is continuum modeling [16]. After this voltage is released, the beams elastic properties will cause the CNT to return to its undeformed position [32]. Dequesnes and Aluru [14] reported that the dynamic pull-in voltage of nano-switches is smaller than the static pull-in voltage, and that the van der Waals force had an significant effect on the pull-in voltage. Due to the pull-in time analysis, the switching frequency ranges from tens to hundreds of GHz. Dequesnes et al. [13] also indicated that fixed–fixed switches were less sensitive to van der Waals force than cantilevers. Numerical simulation showed a closed match with the experimental data. Mahdavi et al. [23] investigated the amplitude frequency response of free vibration of double-walled carbon nanotube (DWCNT). They used both Euler–Bernoulli and Timoshenko models, and showed that van der Waals forces have a significant effect on the response. They also reported the influence of length to outer diameter ratio on the response.

Methods used to investigate the nonlinear dynamics of micro- and nano-electromechanical systems (M/NEMS) reported in the literature include the Method of Multiple Scales (MMS) and the reduced order model (ROM) method. These methods are used to predict the frequency and voltage responses of

electrostatically actuated CNT. Hajnayeb and Khadem [20] reported the behavior of double-walled CNTs bridges under AC and DC voltage actuation with the excitation frequency near natural frequency and twice natural frequency. Both MMS and ROM showed a hardening behavior for low DC voltage and a softening behavior for high DC voltage in the frequency response, and supercritical and subcritical bifurcations in the voltage response, respectively. Ouakad and Younis [30] investigated clamped–clamped CNTs with a certain level of slackness, and DC voltage actuation. They showed that increasing the level of the initial curvature increases the amplitude, and decreases the pull-in DC voltage. Rasekh et al. [31] used ROM to simulate the static and dynamic behavior to include the pull-in phenomenon of CNT bridges under DC and AC voltage actuation. The increase of the initial gap distance resulted in an increase of the pull-in voltage. The pull-out phenomenon was prevented for gaps less than 1 nm due to van der Waals forces. They reported that softening behavior was due to electrical actuation, and hardening behavior was due to the stretching of the neutral axes of CNT. Ghayesh et al. [19] also used ROM to examine the nonlinear behavior of MEM cantilever under AC and DC actuation. The system reported a hardening effect for the frequency response in the cases of primary resonance and superharmonic resonance. Nayfeh and Younis [28] used ROM to analyze the pull-in phenomenon of MEMs under DC and AC actuation for low-voltage MEM switches. They reported both frequency and voltage responses. Both methods MMS and ROM were used to investigate primary and parametric resonance of electrostatically actuated MEMS resonators [4–10].

Voltage response of electrostatically actuated CNTs consists of voltage-amplitude relationship of the resonator. When a DC voltage is applied across a CNT electrode, the cantilever CNT simply deflects, whereas if an AC voltage is applied, the cantilever CNT oscillates [21]. Pull-in voltage characteristics of several nanotube-based electromechanical switches are reported in the literature. For this a continuum model for coupled energy domains, including: the elastostatic, electrostatic, and the van der Waals, was used. In a comparison with atomistic simulations, numerical simulations based upon continuum models closely matched the experimental data [13]. It can further be concluded that the magnitude of the pull-in voltage can be directly affected by the amount of van der Waals forces present. Resonances can lead to complex nonlinear dynamics phenomena, such as hysteresis, dynamic pull-in, hardening and softening behaviors, and frequency bands with an inevitable escape from a potential well [29]. Voltage-amplitude response of electrostatically actuated MEMS cantilevers under soft AC actuation was reported in the literature [6]. They used MMS and ROM (AUTO-07p). A good agreement between MMS and five terms ROM results for amplitude less than half the gap has been reported. Also the convergence of the ROM due to increasing the number of modes of vibration considered has been showed. Chaterjee and Pohit [11] used ROM for voltage-amplitude response of MEMs cantilever under DC and AC voltage actuation.

This paper deals with the voltage response of primary resonance of electrostatically actuated CNT cantilevers. To the best of our knowledge this the first time when (1) the reduced order model (ROM) method [7] is used for investigating electrostatically actuated CNT cantilevers, (2) the convergence of the ROM by using two, three, four and five terms models is reported, and (3) the dimensionless bifurcations and pull-in voltages of the primary resonance of electrostatically actuated CNTs are found. (4) The effects of damping, voltage and van der Waals forces on the voltage response are reported as well.

2 Differential equation of motion

Consider an electrostatically actuated SWCNT cantilever over a parallel ground plate, Fig. 1. A soft AC voltage between the SWCNT and the plate actuates the

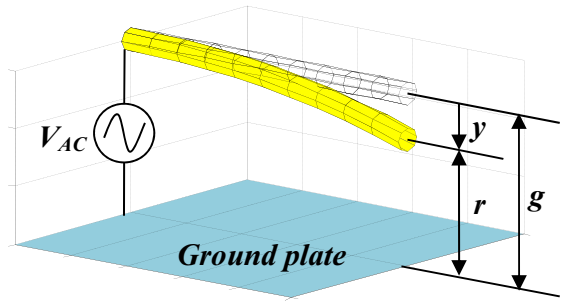

Fig. 1 CNT cantilever under electrostatic, damping and van der Waals forces

SWCNT and leads it into vibration. Three forces act on the SWCNT cantilever (a) electrostatic, due to the soft AC voltage of frequency near half natural frequency of the CNT, (b) van der Waals, and (c) damping. The dimensionless equation of motion is given by [7]

$$\frac{\partial^2 w}{\partial \tau^2} + \frac{\partial^4 w}{\partial z^4} = -b^* \frac{\partial w}{\partial \tau} + \delta \overline{f}_{elec} \cos^2 \Omega^* \tau + \mu \overline{f}_{vdw} \quad (1)$$

where the dimensionless variables w deflection, z longitudinal coordinate, τ time are

$$w = \frac{y}{g};\ z = \frac{x}{\ell};\ \tau = \frac{t}{\ell^2}\sqrt{\frac{EI}{\rho A}} \quad (2)$$

and where the corresponding dimensional variables are y transverse displacement, x longitudinal coordinate, and t time. The dimensionless damping coefficient b^*, dimensionless excitation (voltage) coefficient δ, dimensionless van der Waal coefficient μ, and dimensionless AC frequency Ω * are respectively given by

$$b^* = b\frac{\ell^2}{\sqrt{\rho A E I}}\ ,\ \delta = V_0^2 \frac{\pi \varepsilon_0 \ell^4}{EIg^2}$$
$$\mu = \frac{C_6 \sigma^2 \pi^2 R \ell^4 g^4}{2EIg^{10}}\ ,\ \Omega* = \Omega \ell^2 \sqrt{\frac{\rho A}{EI}} \quad (3)$$

where ρ is mass density, A cross-section area, E Young's modulus, I cross-section moment of inertia, ℓ CNT length, b viscous damping per unit length, ε_0 is the permittivity of the space between the CNT and the ground plate, V_0 is the peak voltage of the applied AC voltage $V(t) = V_0 \cos(\Omega t)$, Ω is the AC frequency of actuation, r the distance between the current position of CNT and the ground plate, R the radius of CNT, Fig. 1. Also, C_6 is a constant characterizing the interactions between the atoms, and σ_0 is the material surface density [13, 14] Table 1. The cross-section moment of inertia of the CNT can be written as $I = \pi\left(R_{ext}^4 - R_{\text{int}}^4\right)/4$ where R_{ext} and R_{int} are the exterior interior radii of CNT, respectively. The relationship between the distance r between the CNT and the ground plate, and the transverse deflection y of the CNT is given by

$$r = g - R - y \quad (4)$$

The dimensionless electrostatic and van der Waals forces in Eq. (1) are as follows

$$\overline{f}_{elec} = \left[(1-w)^2 - s^2\right]^{-\frac{1}{2}} \times \log^{-2}\left(\frac{1-w}{s} + \sqrt{\frac{(1-w)^2}{s^2} - 1}\right) \quad (5)$$

$$\overline{f}_{vdw} = \frac{\left[8\ (1-w-s)^4 + 32(1-w-s)^3 s + 72\ (1-w-s)^2 s^2 + 80\ (1-w-s)s^3 + 35\ s^4\right]}{\left[(1-w)^2 - s^2\right]^{\frac{9}{2}}} \quad (6)$$

where $s = R/g$. The electrostatic force was computed using the classical capacitance model. "The capacitance per unit length for a cylindrical beam over a conductive ground plane was used to determine the dimensional electrostatic force per unit length" [13]. The van der Waals force was computed for a SWCNT and a single monolayer of graphite as ground plane. The van der Waals force was derived from the Waals energy which has been modeled by the Lenard-Jones potential. The total van der Waals energy was computed as an integral over the surfaces of a shell and the plane graphene of the Lenard-Jones potential,

Table 1 Constants

Symbol	Description	Value (unit)
ε_0	Permittivity of vacuum	8.85×10^{-12} C^2/N/m^2
C_6	Material constant	2.43×10^{-78} Nm^7
σ	Graphite surface density	3.80×10^{19} m^{-2}
E	Young modulus	1.20×10^{12} N/m^2
ρ	Density	1.40×10^{3} kg/m^3

[13]. Van der Waals force cannot be neglected for gap distance less than 50 nm. The frequency of AC is near half natural frequency $\Omega^* \cong \omega_k/2$, and can be written as

$$\Omega^* = \frac{\omega_k}{2} + \varepsilon\sigma \tag{7}$$

where σ is frequency detuning parameter, ε book-keeping device, and ω_k dimensionless natural frequency ($\bar{\omega}_k$ is the corresponding dimensional natural frequency) given by

$$\omega_k = \bar{\omega}_k \ell^2 \sqrt{\frac{\rho A}{EI}} \tag{8}$$

Damping force depends on the environment in which the CNT cantilever system is vibrating. It is assumed a viscous damping environment [4], therefore linear damping.

3 Reduced order model (ROM) method

In order to conserve all singularities of the system, the electrostatic and van der Waals forces are expanded in Taylor series in their denominators and the first 8 terms from each expansion are kept. Equation (1) becomes [7]

$$\frac{\partial^2 w}{\partial \tau^2} + b^* \frac{\partial w}{\partial \tau} + \frac{\partial^4 w}{\partial z^4} = \mu \frac{1}{\sum_{i=0}^{7} \lambda_i w^i} + \delta \cos^2 \Omega^* \tau \frac{1}{\sum_{j=0}^{7} \alpha_j w^j} \tag{9}$$

Multiplying Eq. (9) by its both denominators, it results

$$\left(\frac{\partial^2 w}{\partial \tau^2} + b^* \frac{\partial w}{\partial \tau} + \frac{\partial^4 w}{\partial z^4}\right) \sum_{i=0}^{7} \lambda_i w^i \sum_{j=0}^{7} \alpha_j w^j = \mu \sum_{j=0}^{7} \alpha_j w^j + \delta \sum_{i=0}^{7} \lambda_i w^i \cos^2 \Omega^* \tau \tag{10}$$

ROM method is used to solve Eq. (10) for the CNT cantilever. The solution of transverse deflection of CNT is approximated by

$$w(\tau, z) = \sum_{k=1}^{N} u_k(\tau) \varphi_k(z) \tag{11}$$

where $u_k(\tau)$ and $\varphi_k(z)$ are the kth time varying generalized coordinate and the kth linear undamped mode shape of the uniform tube, respectively. N is the number of terms considered in ROM. Substituting Eq. (11) into Eq. (10) and using the followings

$$\begin{aligned} \frac{\partial^2 w(\tau, z)}{\partial \tau^2} &= \sum_{k=1}^{N} \ddot{u}_k(\tau) \varphi_k(z), \\ \frac{\partial w(\tau, z)}{\partial \tau} &= \sum_{k=1}^{N} \dot{u}_k(\tau) \varphi_k(z), \\ \frac{\partial^4 w(\tau, z)}{\partial z^4} &= \sum_{k=1}^{N} \omega_k^2 u_k(\tau) \varphi_k(z) \end{aligned} \tag{12}$$

where ω_k is the kth natural frequency of the CNT, and then multiplying the resulting equation by φ_n, $n = 1,2,\ldots,N$, and integrating with respect to z from 0 to 1, N ROM 2nd order differential equations result as follows

$$\begin{aligned} &\left(\alpha_0 \lambda_0 g_n + \sum_{p=1}^{7} \sum_{i=1}^{p} \alpha_i \lambda_{p-i} \sum_{n, j1, j2, \ldots, j(p-i)}^{N} u_{j1} u_{j2} \ldots u_{j(p-i)} g_{n, j1, j2, \ldots, j(p-i)} \right. \\ &\qquad \left. + \sum_{p=1}^{7} \sum_{i=p}^{7} \alpha_i \lambda_{7+p-i} \sum_{j1, j2, \ldots, j(p+7)}^{N} u_{j1} u_{j2} \ldots u_{j(p+7)} g_{n, j1, j2, \ldots, j(p+i)} \right) \cdot \\ &\left(\sum_{j1}^{N} \ddot{u}_{j1} + b^* \sum_{j1}^{N} \dot{u}_{j1} + \sum_{j1}^{N} \omega_{j1}^2 u_{j1} \right) \\ &= \sum_{p=0}^{7} \left(\alpha_p \delta \cos^2 \Omega^* \tau + \mu \lambda_p \right) \sum_{n, j1, j2, \ldots jp}^{N} u_{j1} u_{j2} \ldots u_{jp} g_{n, j1, j2, \ldots jp} \end{aligned} \tag{13}$$

where the coefficients $g_{n,j1,j2,\ldots jp}$ are given by

$$g_{n,j1,j2,\ldots jp} = \int_0^1 \varphi_n \varphi_{j1} \varphi_{j2} \ldots \varphi_{jp} dz \tag{14}$$

The system of differential equations (13) is transformed into a system of 2 N first order differential equations to be solved. For example, two terms ROM is transformed into four first order differential equations as follows

$$\begin{aligned} y(1) &= u_1 \Rightarrow \dot{y}(1) = y(2) \\ y(2) &= \dot{u}_1 \Rightarrow \dot{y}(2) = \ddot{u}_1 \\ y(3) &= u_2 \Rightarrow \dot{y}(3) = y(4) \\ y(4) &= \dot{u}_2 \Rightarrow \dot{y}(4) = \ddot{u}_2 \end{aligned} \tag{15}$$

In this work, the number of terms of the ROM is $N = 2,\ldots,5$.

The ROM system of the resulting *2 N* first order non-explicit-coupled differential equations is solved using AUTO 07P [15], a continuation and bifurcation software for ordinary differential equations.

4 Numerical simulations

The voltage-amplitude response of the electrostatically actuated CNT is investigated by conducting numerical simulations for a typical CNT. Dynamic modal characteristics of a cantilever to be used in the ROM consist of natural frequencies and mode shapes and they are given

$$\begin{aligned} \varphi_k(z) = &\cosh(\sqrt{\omega_k}x) - \cos(\sqrt{\omega_k}x) \\ &- c_k[\sinh(\sqrt{\omega_k}x) - \sin(\sqrt{\omega_k}x)] \end{aligned} \tag{16}$$

and Table 2. The mode shape functions are orthonormal. The dimensional characteristics of the typical CNT are given in Table 3. Using these values the dimensionless parameters of the system are determined and given in Table 4. The coefficients of the denominator Taylor expansion, see Eqs. (10, 17), are given in Table 5.

Table 3 Dimensional parameters

Symbol	Description	Value (unit)
ℓ	Length of CNT	200×10^{-9} m
R	CNT radius	10^{-9} m
R_{int}	CNT inner radius	0.665×10^{-9} m
g	Gap CNT—plate	20×10^{-9} m
V	Voltage applied	30×10^{-3} V

Table 4 Dimensionless parameters

Symbol	Description	Value
δ	Electrostatic parameter	0.1902
μ	Van der Waals parameter	0.0005
b^*	Damping parameter	0.001

Table 5 Denominator Taylor expansion coefficients Eq. (9) of electrostatic and van der Waals forces

Symbol	Value	Symbol	Value
α_0	13.586202	λ_0	0.1226795
α_1	−20.99676	λ_1	−0.617992
α_2	4.6816821	λ_2	1.2429685
α_3	1.2246554	λ_3	−1.247656
α_4	0.5279667	λ_4	0.6249998
α_5	0.2830802	λ_5	−0.125001
α_6	0.15756904	λ_6	−0.00000049
α_7	0.10349291	λ_7	−0.00000044

In this work a linear damping is assumed Eq (1). It has been reported in the literature that the drag force per unit length on a cylinder in free-molecular flow [26] becomes linear if the ratio of the cylinder velocity to the thermal velocity of the gas u/c is much smaller than one [25]. As the thermal velocity is given by

Table 2 First five natural frequencies and mode shape coefficients for CNTs

	k = 1	*k = 2*	*k = 3*	*k = 4*	*k = 5*
ω_k	3.51602	22.0345	61.70102	120.91202	199.85929
c_k	−0.734	−1.0185	−0.9992	−1.00003	−1.00000

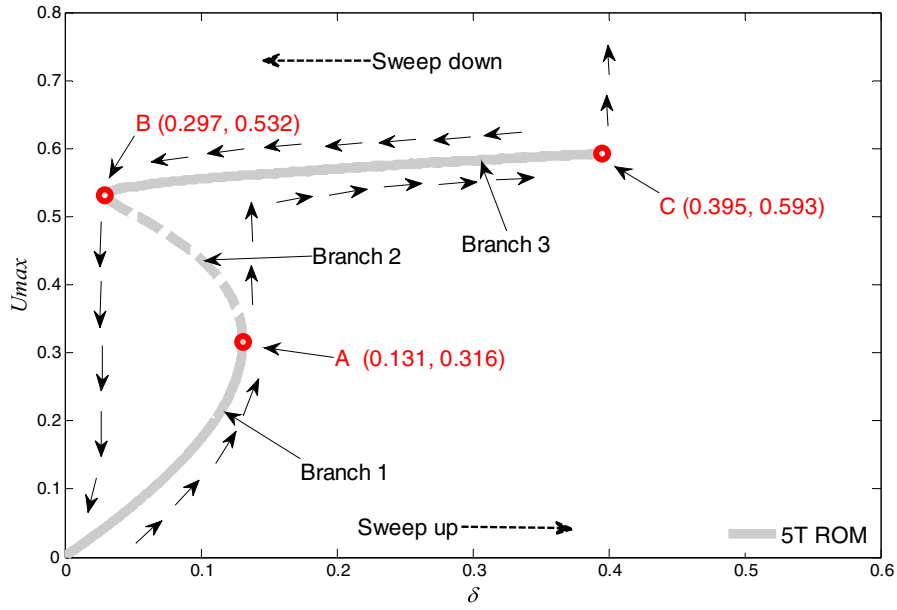

Fig. 2 Voltage–amplitude response AC near half natural frequency by using 5T ROM. $b^* = 0.001$, $\sigma = -0.012$, $\mu = 0.0005$

$c = \sqrt{2k_BT/m_g}$ where $k_B = 1.380648528 * 10^{-23}$ J/K is Boltzman constant, $T = 300$ K is the assumed gas temperature in this work, and $m_g = 48.1 * 10^{-27}$ kg the mass of a gas molecule, then the thermal velocity results as $c = 415$ m/s. On the other hand the dimensionless displacement of the free end of the CNT cylinder can be written as $u = U_{\max} * \cos(\omega_1\tau + \beta)$, [7], where U_{max} is the amplitude of the free end and it is limited to the gap $g = 20$ nm, and $\omega_1 = 3.51602$ is the dimensionless fundamental natural frequency, which can be used to find the dimensional fundamental natural frequency $\bar{\omega}_1$ using Eq. (3) the same formula as for AC frequency. The maximum velocity of the free end can be then found as $u_{\max} = g\bar{\omega}_1$ which gives a value of $u_{\max} = 31$ m/s. Therefore the ratio of the cylinder velocity to the thermal velocity of the gas is $u_{\max}/c = 0.075$ which is much smaller than one, so the linear damping assumption holds for the investigated CNT primary resonance.

Figure 2 shows the voltage amplitude response of the CNT cantilever. In the horizontal axis is the dimensionless voltage parameter δ, and in the vertical axis is the amplitude U_{max} of the free end of the CNT. There is a limited range of the voltage parameter (<0.4, Fig. 2) for which the CNT does not undergo a pull-in phenomenon (contact with the ground plate $U_{max} = 1$). Three distinct branches, two stable and one unstable, are showed. Stable branches are represented by solid lines and the unstable branch by dash line. As the voltage is swept up, the amplitude increases along branch 1 until it reaches the bifurcation point A (0.131, 0.316), where the CNT loses stability and jumps to an amplitude of $U_{max} = 0.56$ on branch 3. As the voltage continues to be swept up, the amplitude increases along branch 3 until it reaches point C (0.395, 0.593), where it loses stability and the amplitude suddenly increases until the CNT goes into pull-in. This is showed by the arrows below the branches and oriented to the right-hand side and up. If the initial amplitude of the CNT is on branch 3 and the voltage is swept down, the amplitude decreases along branch 3 until reaches point B (0.297, 0.532), where it loses stability and jumps to a lower amplitude of $U_{max} = 0.047$ on branch 1. Then, as the voltage continues to be swept down to zero, the amplitude U_{max} decreases to zero. This is showed by the arrows above the branches and oriented to the left-hand side and down.

5 Discussion and conclusions

Figure 3 illustrates the convergence of the voltage-amplitude response with respect to the number of terms $N = 2,3,4$ and 5 of ROM. One can notice the convergence of the method. While the response in amplitudes below $U_{max} = 0.2$ (20 % of the gap) does

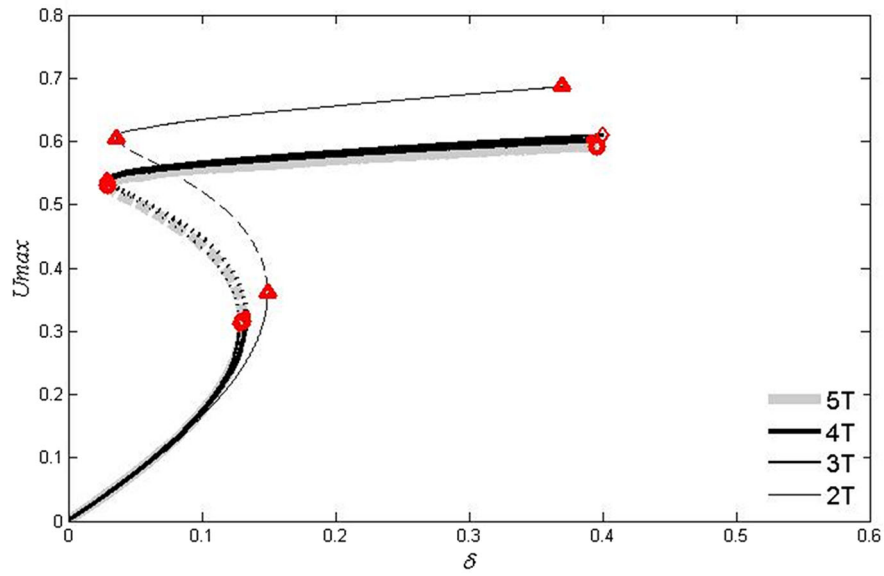

Fig. 3 ROM convergence for the voltage-amplitude response by using two terms (2T), 3T, 4T, and 5T ROM. $b* = 0.001$, $\sigma = -0.012$, $\mu = 0.0005$

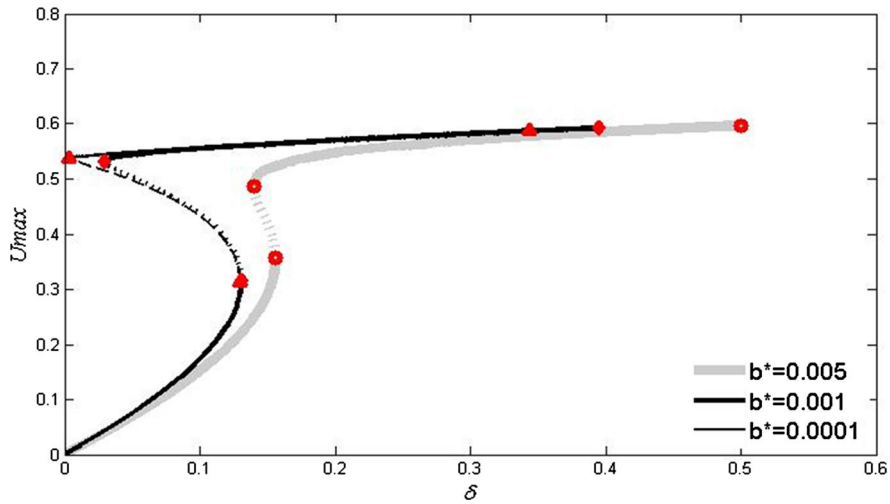

Fig. 4 Influence of damping on the voltage response by using 5T ROM. $\sigma = -0.012$, $\mu = 0.0005$

not depend on the number of terms, for larger amplitudes the number of terms becomes significant. Using only two terms in the ROM leads to overestimating both the amplitude and voltage of the bifurcation point *A*, overestimating the amplitude of the bifurcation point *B* and the amplitude of pull-in point *C,* and underestimating the pull-in voltage of point *C*. Therefore, for reliable results five terms should be considered in the ROM.

Figure 4 shows the effect of dimensionless damping parameter b^* on the voltage-amplitude response. Damping does not have significant effect on the large amplitudes of the cantilever, which are about 0.55 of the gap. However, the larger the damping, the larger the pull-in voltage of point *C* and the larger the bifurcation voltages of bifurcation points *A* and *B*. Also, increasing damping decreases the difference between the voltages of bifurcation points *A* and *B,* jump up and jump down voltages.

Figure 5 illustrates the effect of dimensionless van der Waals force parameter μ on the voltage-amplitude response. As the value of the van der Waals parameter increases, (1) the amplitude of the pull-in point *C* decreases, while (2) the voltage of pull-in point

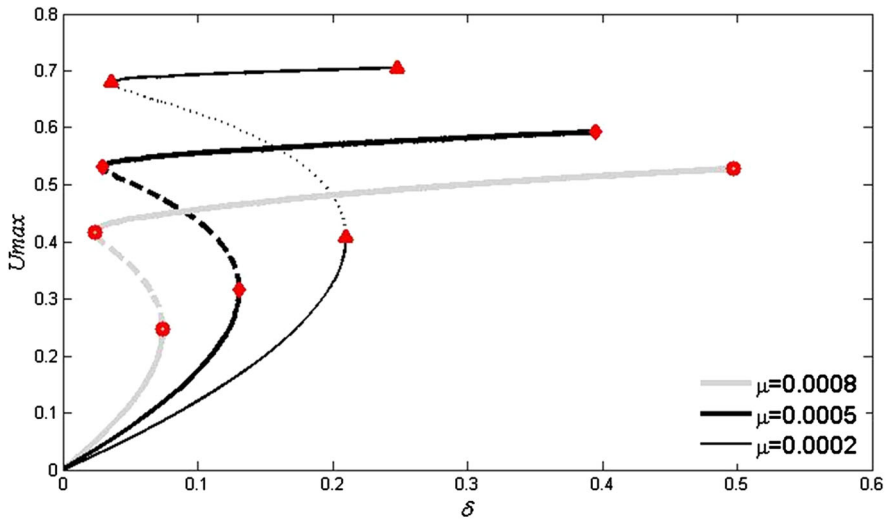

Fig. 5 Influence of van der Waals force on the voltage response by using 5T ROM. $b^* = 0.001$, $\sigma = -0.012$

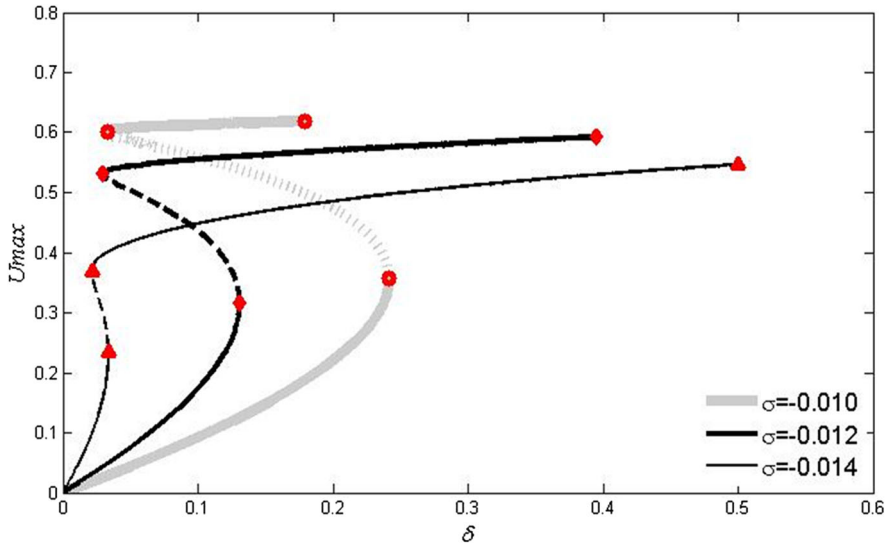

Fig. 6 Influence of frequency on the voltage response by using 5T ROM. $b^* = 0.001$, $\mu = 0.0005$

C increases, and (3) the bifurcation points *A* and *B* shift to lower amplitude and voltage values, i.e. the jump phenomenon occurs at lower amplitude and voltage values.

Figure 6 shows the effect of dimensionless detuning frequency parameter σ on the voltage-amplitude response. As the detuning frequency is increasing towards the resonance frequency, (1) the nonlinear behavior of the system is strengthened, and (2) the amplitude and voltage values of the bifurcation points *A* and *B* increase, i.e. the jump up phenomenon at point *A* occurs at higher voltage and larger amplitude if larger frequency. One can notice that in the case of $\sigma = -0.010$ the CNT goes into pull-in directly from bifurcation point *A*, while for the other two frequencies, the amplitude jumps to larger amplitudes, and then to pull-in as the voltage is swept up. (3) The amplitude of pull-in instability point *C* increases and its voltage decreases.

One should mention that "Casimir force is not included in this model because it is not present for such small gaps as in this work. Casimir force and van der Waals force cannot act at the same time since they describe the same physical phenomenon at different

scales (gap values), Batra et al. [2]. While van der Waals force models the phenomenon for gaps below 50 nm, Casimir force acts for gaps between 200 nm and 1 μm. In between is a transition between van der Waals force and Casimir force," [7].

This work is limited in terms of numerical simulations to the convergence of the voltage-amplitude response with respect to the number of terms $N = 2, 3, 4$ and 5 of ROM, and the use of 5 terms ROM for effects of various parameters. It does not address the influence of the parametric errors in this approach.

Aknowledgements This work was supported by the National Science Foundation under DMR Grant # 0934157 (PREM-The University of Texas Pan American/University of Minnesota—Science and Engineering of Polymeric and Nanoparticle-based Materials for Electronic and Structural Applications).

References

1. Arun A, Acquaviva D, Fernandez-Bolanos M, Salet P, Le-Poche H, Pantigny P et al (2010) Carbon nanotube vertical membranes for electrostatically actuated micro-electro-mechanical devices. Microelectron Eng 87(5–8):1281–1283
2. Batra R, Porfiri M, Spinello D (2008) Reduced-order models for microelectromechanical rectangular and circular plates incorporating the Casimir effect. Int J Solids Struct 45:3558–3583
3. Bhushan A, Inamdar MM, Pawaskar DN (2014) Simultaneous planar free and forced vibrations analysis of an electrostatically actuated beam oscillator. Int J Mech Sci 82:90–99
4. Caruntu DI, Knecht MW (2011) On nonlinear response near half natural frequency of electrostatically actuated microresonators. Int J Struct Stab Dyn 11(4):641–672
5. Caruntu DI, Martinez I, Taylor KN (2013) Voltage-amplitude response of alternating current near half naturalf electrostatically actuated MEMS resonators. Mech Res Commun 52(1):25–31
6. Caruntu DI, Martinez I, Knecht MW (2013) ROM analysis of frequency response of AC near half natural frequency electrostatically actuated MEMS cantilevers. J Comput Nonlinear Dyn 8(1):031011-1
7. Caruntu DI, Luo L (2014) Frequency response of primary resonance of electrostatically actuated CNT cantilevers. Nonlinear Dyn 78(3):1827–1837
8. Caruntu DI, Taylor KN (2014) Bifurcation type change of AC electrostatically actuated MEMS resonators due to DC bias. Shock Vib 2014: Article ID 542023
9. Caruntu DI, Martinez I (2014) Reduced order model of parametric resonance of electrostatically actuated MEMS cantilever resonators. Int J Non-Linear Mech 66(1): 28–32
10. Caruntu DI, Knecht MW (2015) Microelectromechanical systems cantilever resonators under soft alternating current voltage of frequency near natural frequency. J Dyn Syst Meas Contr 137:041016-1
11. Chaterjee S, Pohit G (2009) A large deflection model of the pull-in analysis of electrostatically actuated microcantilever beams. J Sound Vib 322:969–986
12. Chowdhury R, Adhikari S (2009) Vibrating carbon nanotube based bio-sensors. Physica E 42:104–109
13. Dequesnes M, Rotkin SV, Aluru NR (2002) Calculation of pull-in voltages for carbon-nanotube-based nanoelectromechanical switches. Nanotechnology 13:120–131
14. Dequesnes M, Aluru NR (2004) Static and dynamic analysis of carbon nanotube-based switches. J Eng Mater Technol 126:230–237
15. Doedel EJ, Oldeman BE (2009) AUTO-07P: continuation and bifurcation software for ordinary differential equations. Concordia University, Montréal
16. Fakhrabadi MS, Khorasani PK, Rastgoo A, Ahmadian MT (2013) Molecular dynamics simulation of pull-in phenomena in carbon nanotubes with Stone-Wales defects. Solid State Commun 157:38–44
17. Fakhrabadi MS, Rastgoo A, Ahmadian MT (2014) Size-dependent instability of carbon nanotubes under electrostatic actuation using nonlocal elasticity. Int J Mech Sci 80:144–152
18. Georgantznos SK, Anifantis NK (2010) Carbon nanotube-based resonant nanomechanical sensors: A computational investigation of their behavior. Physica E 42:1795–1801
19. Ghayesh MH, Farokhi H, Amabili M (2013) Nonlinear behavior of electrically actuated MEMS resonators. Int J Eng Sci 71:137–155
20. Hajnayeb A, Khadem SE (2012) Nonlinear vibration and stability of a double-walled carbon nanotube under electrostatic actuation. J Sound Vib 331:2443–2456
21. Kaul AB, Wong EW, Epp L, Hunt BD (2006) Electromechanical carbon nanotube switches for high frequency applications. Nano Lett 5(6):942–947
22. Liang F, Su Y (2013) Stability analysis of a single-walled carbon nanotube conveying pulsating and viscous fluid with nonlocal effect. Appl Math Model 37(10–11):6821–6828
23. Mahdavi MH, Jiang LY, Sun X (2011) Nonlinear vibration of a double-walled carbon nanotube embedded in a polymer matrix. Physica E 43:1813–1819
24. Malik R, Alvarez N, Haase M, Ruff B, Song Y, Suberu B, et al (2014) Carbon nanotube sheet: processing, characterization and applications. In: Shanov VN, Yin Z, Schulz MJ (eds) Nanotube super-fiber materials, Elsevier, pp 349–387
25. Martin MJ, Houston BH (2007) Gas damping of carbon nanotube oscillators. Applied Physics Letters 91:103116-1–3
26. Maslach GJ, Schaaf SA (1963) Cylinder drag in the transition from continuum to free-molecule flow. Phys Fluids 6(3):315–321
27. Mehdipour I, Erfani-Moghadam A, Mehdipour C (2013) Application of an electrostatically actuated cantilevered carbon nanotube with an attached mass as a bio-sensor. Curr Appl Phys 13(7):1463–1469
28. Nayfeh AH, Younis MI (2007) Dynamics pull-in phenonmeon in MEMs resonators. Nonlinear Dyn 48:153–163
29. Ouakad HM, Younis MI (2009). Nonlinear dynamics of electrically actuated carbon nanotube resonators. 2008 Proceedings of the ASME international mechanical

engineering congress and exposition, vol 11, pp 791–798
30. Ouakad HM, Younis MI (2011) Natural frequencies and mode shapes of initially curved carbon nanotube resonators under electric actuation. J Sound Vib 330:3182–3195
31. Rasekh M, Khadem SE, Tatari M (2010) Nonlinear behavior of electrostatically actuated carbon nanotube-based devices. J Phys D Appl Phys 43(315301):1–10
32. Rasekh M, Khadem SE (2011) Pull-in analysis of an electrostatically actuated nano-cantilever beam with nonlinearity in curvature and inertia. Int J Mech Sci 53(2):108–115
33. Souayeh S, Kacem N (2014) Computational models for large amplitude nonlinear vibrations of electrostatically actuated carbon nanotube-based mass sensors. Sens Actuators, A 208:10–20
34. Wu DH, Chien WT (2006) Resonant frequency analysis of fixed-free single-walled carbon nanotube-based mass sensor. Sens Actuator A: Phys 126:117–121
35. Zhang R, Zhang Y and Wei F (2014) Synthesis and properties of ultralong carbon nanotubes. In: Shanov VN, Yin Z, Schulz MJ (eds) Nanotube Superfiber Materials, Elsevier, pp 87–136